Text submitted to the Journal of Applied Physics for publication

Properties of single crystalline semiconducting $CoSb_3$

T. Caillat[a], A. Borshchevsky, and J.-P. Fleurial

Jet Propulsion Laboratory
California Institute of Technology
4800 Oak Grove Drive, MS 277/207
Pasadena, CA 91109
[a] e-mail: thierry.caillat@jpl.nasa.gov

ABSTRACT

A study of the properties of the skutterudite compound $CoSb_3$ was carried out on single crystals grown by the Bridgman gradient freeze technique. P- and n-type samples were obtained over a wide range of carrier concentration. As-grown crystals show p-type conductivity and n-type samples were obtained by addition of Te or Pd. Samples were characterized by X-ray diffractometry, microprobe analysis and density measurements. A number of physical properties of $CoSb_3$ such as linear thermal expansion coefficient, sound velocity, and Debye temperature were determined and are presented. Seebeck coefficient, electrical resistivity, thermal conductivity, and Hall effect measurements were performed between room temperature and about 900K. Exceptionally high Hall mobilities were obtained on p-type samples with a maximum room temperature Hall mobility of 3,300 $cm^2 V^{-1} s^{-1}$ at a carrier concentration of 1×10^{17} cm^{-3}. Our results show that the dominant carrier scattering mechanism around room temperature is acoustic phonon scattering. The results of the transport property measurements are discussed and compared to recent predictions based on band structure calculations. It was found that a model based on a single parabolic band with acoustic phonon scattering can satisfactorily describe the transport properties of $CoSb_3$. The potential of $CoSb_3$ for thermoelectric applications is also discussed.

INTRODUCTION

$CoSb_3$ belongs to a broad family of materials with the skutterudite structure which have been recently identified as potential new thermoelectric materials.[1-3] The skutterudite structure is composed of a cubic lattice, space group *Im3*, and the unit cell contains 8 $CoSb_3$ groups. $CoSb_3$ decomposes peritectically at 1146K.[4] A band gap of about 0.5 eV was estimated for $CoSb_3$ by Dudkin and Abrikosov[5] from high temperature electrical resistivity measurements on polycrystalline samples. Optical measurements performed on a crystal of $CoSb_3$ grown by a vapor transport technique revealed a metallic behavior.[6] More recently, measurements of the low temperature transport properties of p-type

$CoSb_3$ single crystals were reported[7] and band structure calculations were performed for $CoSb_3$ by Singh and Pickett.[7] These calculations revealed some unusual band structure features for $CoSb_3$ and other skutterudite binary compounds. It was found that, in the compounds $CoAs_3$, $CoSb_3$, and $IrSb_3$, a single band crosses the pseudogap, touching the minimum of the conduction band in $IrSb_3$ and $CoAs_3$ and nearly doing so in $CoSb_3$. In addition, the gap-crossing band has a linear behavior for $CoSb_3$ and $IrSb_3$. As a result, the transport properties of $CoSb_3$ are expected to be significantly different from standard semiconductor behavior. Singh and Pickett[7] predicted that, for doping levels as low as 3×10^{16} cm^{-3}, the properties are determined by the linear dispersion. In the constant scattering time approximation, the hole mobility (μ_p) would vary as $p^{-1/3}$, where p is the carrier concentration. Singh and Pickett[7] calculated for $CoSb_3$ a direct band gap and an indirect band gap of 0.57 and 0.8 eV, respectively.

In a recent study of a lightly doped $CoSb_3$ crystal grown by a flux method, Mandrus *et al.*[8] could not confirm some of the predictions of Singh and Pickett.[7] In particular, they concluded that the hole mobility was unlikely to vary as $p^{-1/3}$. In order to further investigate the properties of $CoSb_3$, we grew n- and p-type single crystals of $CoSb_3$ over a wide range of carrier concentration and measured a number of their properties such as electrical resistivity, Hall coefficient, Seebeck coefficient, and thermal conductivity over a wide range of temperatures. The results are discussed and compared to the predictions of Singh and Pickett.[7] The potential of $CoSb_3$ for thermoelectric applications is also discussed.

EXPERIMENTAL DETAILS

Single crystals of $CoSb_3$ were grown using the gradient freeze technique from Sb-rich melts in sealed quartz ampoules coated with amorphous carbon. Details about the crystal growth can be found elsewhere.[9] As-grown samples always show p-type conductivity and n-type samples were obtained by substituting Sb for Te or Pd at concentrations between 0.1 to 0.2 at.%. Te pieces (99.999%) or Pd powder (99.99%) were introduced in the original melts. Typical ingots were composed of two parts after the growth: the bottom part corresponding to the compound $CoSb_3$ and the upper part corresponding to the Sb-rich eutectic. Large single crystals (up to 10 mm long and 10 mm in diameter) were grown. For p-type samples, the variations of carrier concentration were naturally obtained from the tip to the top of the grown ingots. This is presumably due to the changes of stoichiometric deviations during the growth although we were unable to confirm this by microprobe analysis. N-type samples with different doping levels were obtained by varying the nominal amount of dopants in the melts and also because of the segregation of the dopant during the growth resulted in variations of the carrier concentration along the grown ingots.

Selected samples were polished and their microstructures were investigated under an optical microscope. Microprobe analyses (MPA) were performed on the same samples on a JEOL JXA-733 superprobe to check that the samples were single phase. Some

samples were ground for x-ray diffractometry (XRD) analyses which were conducted on a Siemens D-500 diffractometer with the Cu-K_α radiation. Silicon powder was used as a standard and mixed to the powdered samples. The powder x-ray patterns were taken with scan steps of 2Θ 0.05° and counting time of 3 s. The high temperature x-ray data were also taken on one sample up to about 950K to investigate the temperature dependence of the lattice constant of $CoSb_3$. The density of some samples was measured by the immersion technique using toluene as the liquid. The measured densities were found to be about 99.5% of the theoretical density (7.621 g/cm^3). The shear and longitudinal sound velocity were measured at room temperature on a single crystal of $CoSb_3$ about 8 mm long using a frequency of 5 Mhz.

Samples about 2 mm thick and 10 mm in diameter were cut from the grown ingots for transport property measurements. All samples were characterized at room temperature by Seebeck coefficient, Hall effect and electrical resistivity measurements. The high temperature resistivity, Hall effect, Seebeck coefficient, thermal diffusivity, and heat capacity measurements were conducted on selected samples between room temperature and about 900K. The electrical resistivity (ρ) was measured using the van der Pauw technique with a current of 100 mA using a special high temperature apparatus.[10] The Hall coefficient (R_H) was measured in the same apparatus with a constant magnetic field value of ~ 10000 Gauss. The carrier density was calculated from the Hall coefficient, assuming a scattering factor of 1 in a single carrier scheme, by $p/n = 1/R_H e$ where p and n are the densities of holes and electrons, respectively, and e is the electron charge. The Hall mobility (μ_H) was calculated from the Hall coefficient and the resistivity values by $\mu_H = R_H/\rho$. The errors were estimated at ± 0.5% and ± 2% for the resistivity and Hall coefficient measurements, respectively. The Seebeck coefficient of the samples was measured on the same samples used for resistivity and Hall coefficient measurements using a high temperature light pulse technique.[11] The error of the Seebeck coefficient measurement was estimated to be less than ± 1%. The heat capacity and thermal diffusivity were measured using a flash diffusivity technique[12] and the overall error in the thermal conductivity measurements was estimated at about ± 10%. The thermal conductivity was calculated from the experimental density, heat capacity, and thermal diffusivity values.

II. RESULTS AND DISCUSSIONS

A. Electrical properties

Some room temperature properties of p-type $CoSb_3$ are summarized in Table I and compared to the results of Slack and Tsoukala obtained on a p-type polycrystalline $IrSb_3$ sample.[5] Samples with p-type conductivity were obtained with Hall carrier concentration ranging from 10^{17} cm^{-3} to about 10^{19} cm^{-3} and n-type samples ranging from about 10^{18} cm^{-3} to 10^{21} cm^{-3}. The room temperature Hall mobility values for p- and n-type $CoSb_3$ crystals are plotted in Fig. 1 as a function of the carrier concentration. In agreement with several previous studies of skutterudite materials, $CoSb_3$ samples exhibit very large hole

mobility values in the carrier concentration range investigated, reaching a maximum of about 3,300 $cm^2 V^{-1} s^{-1}$ at the lowest carrier concentrations. The variation of the hole mobility with carrier concentration can be divided into two regions: the first region between 10^{17} and 10^{18} cm^{-3} where the hole mobility varies little and a second region, at higher carrier concentrations, where the hole mobility decreases with increasing carrier concentration. A similar behavior was observed for the narrow gap semiconductor Sb_2Te_3[13] and was explained by the presence of two different valence bands. N-type samples have much lower mobility values with a maximum of about 200 $cm^2 V^{-1} s^{-1}$ at a carrier concentration of about 10^{18} cm^{-3}. This suggests a strong dissimilitude between the conduction and valence band (s) in this material. The room temperature electrical resistivity values are shown in Fig. 2 for n- and p-type crystals. As a result of the large difference in hole and electron mobility in this material, the electrical resistivity of n-type samples is about 25 times larger than for p-type samples at a given carrier concentration. A resistivity value of 1mΩcm (this is about the optimal value for which maximum thermoelectric figure of merits are obtained for state-of-the-art thermoelectric materials) can be obtained at a carrier concentration of $3x10^{18}$ cm^{-3} for the p-type and of $2x10^{20}$ cm^{-3} for the n-type.

The room temperature Seebeck coefficient values are presented in Fig. 3. N-type samples have much larger Seebeck coefficient values than p-type, at a given carrier concentration. The larger n-type Seebeck coefficient are presumably due to larger carrier effective masses. We present in Fig. 4 the room temperature values for the power factor ($PF = \alpha^2/\rho$) which is used to calculate the thermoelectric figure of merit Z defined as $Z = \alpha^2/\rho\lambda = PF/\lambda$. The maximum values for the power factor are about 30 $\mu W cm^{-1} K^{-2}$ for both n- and p-type $CoSb_3$ but the maxima occurs at different carrier concentrations. For n-type, there appears to be a maximum in the values at a carrier concentration of about $2x10^{20}$ cm^{-3} but it is no clear yet if, by increasing the carrier concentration of p-type samples higher than 10^{19} cm^{-3}, larger power factor values could be obtained. A simple extrapolation using fits of the Seebeck coefficient and electrical resistivity values shows that larger values might be achieved. Efforts to prepare more heavily doped p-type samples would be worthy to assess the veracity of this prediction.

We measured the electrical resistivity, Hall coefficient, and Seebeck coefficient of several n- and p-type $CoSb_3$ crystals from room temperature up to about 900K. The room temperature properties of these samples are listed in Table II. The low temperature data for $CoSb_3$ single crystals were presented elsewhere.[5]

The variations of the electrical resistivity and Hall coefficient as a function of inverse temperature are shown for p-type $CoSb_3$ crystals in Fig. 5 and 6, respectively. For the more heavily doped p-type samples, the electrical resistivity increases with increasing temperature up to about 600K where the rise becomes smaller, almost temperature independent. For the lightly doped sample (121OB22), the variations of the resistivity can be divided into four different regions: (1) a small increase from room temperature up to about 350K, (2) a sharp decrease from 350 up to 600K, (3) another region from 600 to

750K where the electrical resistivity is almost temperature independent, and (4) a small decrease from 750 to 900K. In region 2, the resistivity decreases almost linearly with the temperature with an energy gap of about 0.73 eV. This value is close to the direct band gap of 0.8 eV calculated by Singh and Pickett[7] for $CoSb_3$. For p-type samples, the Hall coefficient rises slowly at low temperatures and then decreases almost linearly at higher temperatures with an energy gap of about 0.63 eV. This is close to the indirect pseudogap calculated by Singh and Pickett.[7] The onset of the decrease is shifted to higher temperatures for the most heavily doped samples. At temperatures above 750K, a sharper decrease in the Hall coefficient is observed similarly to the variation of the electrical resistivity. The variations of the Hall coefficient and electrical resistivity can tentatively be explained as follows. The rise of the Hall coefficient in the low temperature domain might be due to the presence of two valence bands with different effective masses. At low temperatures, the carriers would come from a band occupied with the lighter holes corresponding to the extrinsic domain. When the temperature rises, the holes would progressively occupy the second band filled with heavier holes, resulting in the rise of the Hall coefficient with temperature. Then, the electron contribution to the conduction increases at higher temperatures and intrinsic conduction is observed. In the intrinsic domain, one would expect to observe a steady decrease of the electrical resistivity with temperature but the resistivity flattens up at about 600K which we attribute to the presence of the second valence band being increasingly filled with heavier holes, compensating the effects of minority carriers (electrons). At the highest temperatures of measurements, the Hall coefficient and the electrical resistivity decreases again when the influence of the second band becomes weaker.

The variations of the electrical resistivity and Hall coefficient as a function of inverse temperature are shown for n-type $CoSb_3$ crystals in Fig. 7 and 8, respectively. The samples are n-type at low temperatures and become n-type at higher temperatures. The transition temperature from n-type to p-type gradually increases from the samples with the lowest doping levels to the highest. The results are in agreement with the presence of two valence bands as discussed in the previous paragraph. Indeed, at low temperatures, the Hall coefficient and electrical resistivity are characteristic of extrinsic conduction. Then, when an increasing number of holes are thermally excited (from the band containing the heavier holes), the Hall coefficient changes type and the electrical resistivity decreases almost linearly with the temperature with an energy gap of about 0.55 eV. This is close to the indirect band gap of 0.57 eV calculated by Singh and Pickett[7] and estimated by Dudkin and Abrikosov[5] on n-type polycrystalline samples. At the highest temperatures, the electrical resistivity seems to decrease more slowly which might be due to the fact that the electrons are less compensated by lighter holes at these temperatures.

The carrier mobilities are shown as a function of temperature for p- and n-type in Fig. 9 and 10, respectively. The hole mobility values are large and decrease with increasing temperature. The hole mobility follows reasonably a $T^{-3/2}$ behavior between 300 and 500K which indicates that the predominant carrier scattering mechanism is acoustic phonon scattering. Below 200K, Mandrus *et al.*[8] found a $T^{3/2}$ dependence of the hole mobility on one lightly doped p-type $CoSb_3$ sample and they concluded that the

dominant scattering mechanism for their sample was ionized impurities scattering. Low temperature measurements of the hole mobility on our crystals showed a different behavior and the variations were suggestive of a combination of scattering by phonons between 100 and 300K and neutral impurities below 100K.[2] The $T^{3/2}$ behavior observed by Mandrus *et al.*[8] might be due to the presence of impurities in their sample. Around room temperature, the electron mobility follows reasonably well a $T^{-3/2}$ dependence, also indicating that the dominant carrier scattering mechanism is acoustic phonon scattering.

The Seebeck coefficient values are presented in Fig. 11 as a function of temperature for p-type samples. As expected, the lower the doping levels are, the higher the Seebeck coefficients are. For p-type samples, the variations scale with the variations of the Hall coefficient. The Seebeck coefficient increases with increasing temperatures in the extrinsic region and then decreases due to the increasing number of minority carriers. The presence of a second band containing heavier holes can be observed at temperatures above about 800K (a similar change was observed for the Hall coefficient and electrical resistivity at the same temperature) where the decrease becomes more pronounced. N-type Seebeck coefficient values are shown as a function of temperature in Fig. 12. Again the variations are consistent with a presence of two valence bands and can be explained as follows: at low temperatures the Seebeck coefficients are of n-type and large, corresponding to the extrinsic region. When the conduction by minority carrier increases, the Seebeck coefficient decreases and becomes p-type for lightly doped samples. For the same samples, the p-type Seebeck coefficients then decrease with temperatures up to about 800K where the influence of the second band (containing lighter holes) can be seen, resulting in a smaller decrease of the Seebeck coefficient with the temperature.

The larger n-type Seebeck coefficients are presumably due to larger electron masses. We estimated the effective masses using a single parabolic band model with acoustic phonon scattering which was found to be the predominant carrier scattering mechanism around room temperature as we discussed before. In this model, the Seebeck coefficient can be expressed as:[11]

$$\alpha = \pm \frac{k}{e}\left\{2\frac{F_1(\xi)}{F_0(\xi)} - \xi\right\} \qquad (1)$$

where ξ is the reduced Fermi level and F_x is a Fermi integral of order x.[4] Using the same formalism, the carrier concentration can be expressed as:

$$n/p = \frac{4}{\sqrt{\pi}}\left(\frac{2\pi m^* kT}{h^2}\right)^{3/2} F_{1/2}(\xi) \qquad (2)$$

where m^* is the effective mass and T is the temperature in K. The Fermi levels can be calculated from the experimental Seebeck coefficient values using equation (1) and used, together with the experimental Hall carrier concentration values to calculate the effective

masses from equation (2). The results are shown in Fig. 13 and 14 for the hole and electron effective masses, respectively. The hole effective mass increases with increasing carrier concentration which might also suggests the existence of two valence bands with different holes. Mandrus *et al.*[8] estimated an effective mass of about $0.01 m_0$ on one $CoSb_3$ sample doped at 7×10^{16} cm^{-3} using a similar model but with the assumption that impurities phonon scattering predominates. If we extrapolate our results to lower carrier concentrations (using the best-fit curve in Fig. 13), we would find an effective mass of about 0.05 at this carrier concentration. Although the data for the electron effective are more scattered, the values are about ten times larger than hole effective masses. This is why the n-type Seebeck coefficients are so large. The variations of the electron effective masses seem to be divided into two regions: the first one between 10^{18} and about 10^{20} cm^{-3} where the effective mass is almost carrier concentration independent and the second one where it increases sharply for carrier concentrations above 10^{20} cm^{-3}.

In Fig. 15, we compare at room temperature the variations of the experimental Seebeck coefficient values as a function of the carrier concentration to the calculated values using the model proposed by Singh and Pickett[7]. In their model, the Seebeck coefficient is expressed as:[7]

$$\alpha = \left(\frac{2\pi k^2 T}{3es}\right)\left(\frac{\pi}{3p}\right)^{1/3}, \qquad (3)$$

where s is the slope of the linear dispersing band and is -3.10 eV Å for $CoSb_3$. The calculated values seem to be lower than the experimental one's. The comparison was also made with the high temperature Seebeck coefficient values for three samples. The calculation of the Seebeck coefficient values was limited to the domain where the sample exhibit extrinsic conduction, i.e., where the conduction is only due to holes. The results are shown in Fig. 16. The larger disagreement occurs for lightly doped samples for which the calculated Seebeck coefficient values are overestimated.

The hole mobility values were calculated using a single parabolic valence band model with acoustic phonon scattering. In this model, the hole mobility is given by:[14]

$$\mu_p = \frac{2e}{m_p^*}\tau_{acous}\frac{F_0(\xi)}{F_{1/2}(\xi)}, \qquad (4)$$

where τ_{acous} is the energy independent relaxation time corresponding to acoustic phonon scattering. In the same model, the electrical resistivity is expressed as:[14]

$$\rho = \frac{3\, m^* h^3}{8\pi e^2 (2m^* kT)^{3/2}\tau_{acous} F_0(\xi)}, \qquad (5)$$

τ_{acous} was calculated as a function of the Fermi level ξ from equation (5) using the fitted values of the electrical resistivity and the hole effective mass as a function of the Fermi level. The hole mobility values were then calculated as a function of the Fermi level using the calculated values of τ_{acous} and the fitted values of the hole effective masses. The results are shown in Fig. 17 together with the experimental data. Singh and Pickett[7] predicted that, in the linear dispersion model, the hole mobility should follow a $p^{-1/3}$ variation. Although the $p^{-1/3}$ variation seems to be followed for the more heavily doped samples, the experimental hole mobility values do not follow this behavior for carrier concentrations lower than 4×10^{19} cm^{-3}. The calculated values using the parabolic band model with acoustic phonon scattering is in reasonable agreement with the experimental data in most of the carrier concentration range investigated. It seems therefore that models based on the Boltzmann's transport equation in the relaxation time approximation could be used to model the thermal and electrical properties of $CoSb_3$. Such models could be used to predict the thermoelectric properties of $CoSb_3$ as a function of the doping level and help guide the experimental work to achieve the maximum thermoelectric figure of merit.

B. '1'11('1'11}211 properties

X-ray diffractometry analysis of ground $CoSb_3$ samples show that the samples were single phase with a pattern corresponding to the skutterudite crystal structure. We calculated a room temperature lattice constant of a_o = 9.0345 ± 0.0003 Å. This is in good agreement with the results of Kjekshus and Rakke[15] and also with the results of Mandrus *et al.*[3] The variation of the lattice constant versus temperature is shown in Fig. 18. The lattice constant varies linearly between room temperature and about 930K and the compound does not undergo any phase transformation in this temperature range. A thermal expansion coefficient value of 6.36×10^{-6} K^{-1} was calculated for $CoSb_3$ between 300 and 930K. This value is comparable to a value of 6.6×10^{-6} K^{-1} found for $IrSb_3$.[3]

The measured longitudinal (v_l) and shear (v_s) sound velocities are listed in '1'able 1. The mean sound velocity (v_m) is given by:[16]

$$v_m = \left(\frac{1}{3}\left[\frac{2}{v_s^3} + \frac{1}{v_l^3}\right]\right)^{-1/3} \qquad (6)$$

We calculated a mean sound velocity of 2.934×10^5 cm s^{-1}. The Debye temperature is related to the mean sound velocity by:[16]

$$\Theta = \frac{h}{k}\left[\frac{3n}{4p} \frac{N d}{M'}\right]^{1/3} v_m , \qquad (7)$$

where h and k are the Planck's and Botlzmann's constants, respectively, N the Avogadro's number, d the density, and M' the molecular weight of the solid. We

calculated a 1 Debye temperature of 307K for $CoSb_3$. Slack and Tsoukala calculated a 1 Debye temperature of 308K for $IrSb_3$.[3]

Finally, we will discuss the results of the thermal conductivity measurements shown in Fig. 19. The lattice thermal conductivity of the samples was calculated as follows. The total thermal conductivity is the sum of an electronic contribution (λ_e) and a lattice thermal conductivity (λ_L). The electronic contribution (λ_e) can be calculated using the Wiedemann-Franz law:

$$\lambda_e = LT/\rho \quad , \qquad (8)$$

where L is the Lorenz number. Similarly to the Hall coefficient and Seebeck coefficient, the Lorenz number can be expressed as:[1-4]

$$L = \frac{k^2}{e^2} \frac{3 F_0(\xi) F_2(\xi) - 4 F_1^2(\xi)}{F_0^2(\xi)} \quad . \qquad (9)$$

The reduced Fermi level values, obtained from the experimental Seebeck coefficient values using equation (3), were used to calculate the Lorenz number. λ_e was then calculated as a function of temperature using the calculated Lorenz numbers and the experimental resistivity data. The results are shown in Fig. 19. Most of the heat is conducted by the lattice in this material. The room temperature lattice thermal conductivity depends on the doping levels of the samples. For lightly doped samples, the room temperature lattice thermal conductivity is about 100 mW cm^{-1} K^{-1}, in agreement with previous low temperature measurements of $CoSb_3$ single crystals.[2] For more heavily doped samples, the value drops to about 57 mW cm^{-1} K^{-1}. The temperature dependence of the lattice thermal conductivity varies with the doping level of the samples, becoming smaller for heavily doped samples. The results suggest that electron-phonon scattering is responsible for the large decrease in lattice thermal conductivity in heavily doped samples. This scattering mechanism could not be observed for the most heavily doped p-type (~ 10^{19} cm^{-3}) which is probably not high enough to observe any significant hole-phonon scattering.

The lattice thermal conductivity can be estimated using the formalism developed by Slack and Tsoukala.[3] The theoretical lattice thermal conductivity $\lambda'(\Theta)$ at the Debye temperature is given by:

$$\lambda'(\Theta) = \frac{B \bar{M} \delta \Theta^2}{n^{2/3} \gamma^2} \quad , \qquad (10)$$

where $\bar{M}$ is the average mass of an atom of the crystal, δ^3 is the average volume occupied by an atom, Θ is the Debye temperature, n is the number of atoms per unit cell, γ is the

Grüneisen constant at $T = \Theta$, and $B = 3.04 \times 10^7\ s^{-3}\ K^{-3}$. For $CoSb_3$, $M = 106$ g, $\Theta = 307K$, and $n = 32$. A Grüneisen constant of 0.95 was calculated for $CoSb_3$ using the formalism developed by Slack and Tsoukala.[3] The theoretical lattice thermal conductivity obtained from equation (8) for $CoSb_3$ is 101 mW $cm^{-1}\ K^{-1}$ at room temperature. This is in excellent agreement with the experimental room temperature lattice thermal conductivity of 100 mW $cm^{-1}\ K^{-1}$ for lightly doped samples.

A commonly used parameter to gauge the value of materials for thermoelectric applications is the dimensionless figure of merit ZT. The typical limit to all state-of-the-art thermoelectric materials is $ZT \approx 1$. Skutterudites are promising thermoelectric materials because they possess attractive electrical properties, in particular high carrier mobility. We calculated a maximum ZT value of 0.52 at 600K for an n-type sample doped at about $1.4 \times 10^{20}\ cm^{-3}$. In $CoSb_3$ and other binary skutterudite compounds, including $IrSb_3$[3], the ZT values are limited by their relatively high thermal conductivity values. Therefore, efforts should focus on reducing the lattice thermal conductivity of skutterudites. Several phonon scattering mechanisms, including alloy scattering,[17] charge transfer,[18] and voids filling,[19,20] have been recently identified and were found to be effective in reducing the lattice thermal conductivity of some skutterudite materials. In addition to these mechanisms, we have shown that electron-phonon scattering could be very efficient in reducing the lattice thermal conductivity of these compounds. It is also possible that the same scattering will operate in heavily doped p-type samples.

CONCLUSION

We have investigated the properties of n- and p-type $CoSb_3$ single crystals grown by the gradient freeze technique. Transport property measurements show that $CoSb_3$ exhibits exceptionally high hole mobilities which is consistent with the small hole effective masses. The electron effective masses are much larger, resulting in larger Seebeck coefficient values. The temperature dependence of the Hall mobility indicates that acoustic phonon scattering is the dominant scattering mechanism around room temperature. The $p^{-1/3}$ dependence of the hole mobility on the carrier concentration predicted by Singh and Pickett[7] was not observed experimentally. It was found that a model based on a single parabolic band with acoustic phonon scattering can satisfactorily describe the transport properties of $CoSb_3$. Evidence of electron-phonon scattering was found in heavily doped n-type samples, resulting in a reduction of about 50% in the lattice thermal conductivity of $CoSb_3$ at room temperature. A maximum ZT value of 0.52 was obtained for a heavily doped n-type sample at a temperature of 600K. Skutterudite materials have shown good thermoelectric properties but efforts should now focus on lattice thermal conductivity reduction. Several phonon scattering mechanisms, including free-carrier phonon, were identified to reduce the lattice thermal conductivity in skutterudite materials which offer some promise as new thermoelectrics.

ACKNOWLEDGMENTS

The work described in this paper was carried out a the Jet Propulsion Laboratory/California Institute of Technology, under contract with the National Aeronautics and Space Administration. The authors would like to thank Danny Zoltan and Andy Zoltan for thermoelectric properties measurements, Jim Kulleck for x-ray diffractometry, Paul Carpenter for microprobe analyses and Yoseph Bar-Cohen for sound velocity measurements.

REFERENCES

1. Cail lat, A. Borshchevsky, and J. -1'. Fleurial, Proceedings of the Eleventh International Con ference on Thermoel ectrics, Arlington, Texas, 1993, edited *by* K. R. Rao (University of Texas Press, Arlington, 1993).
2. D. '1'. Morelli, 'J'. Caillat, J. -1'. Fleurial, A. Borshchevsky, .1 Vandersand e, B. Chen, and C. Uher, Phys. Rev, B 51, 9622 (1 995).
3. A, Slack and V. G. Tsoukala, J. Appl. Phys. 76, 1665 (] 994).
4. P. Feschotte and 1). 1 .orin, Journal of the Less-Common Metals **155**, 255 (1 989).
S.],.]). Dudkin and N. Kh. Abrikosov, Sov. Phys. Solid State **3**, 126 (1959).
6. J. Ackermann and A, Weld, J. Phys. Chem. Solids **38**, 1013 (]977),
7. D. J. Singh and W. E. Pickett, Phys. Rev. **B 50**, 11235 (1994).
8. D. Mandrus, A, Migliori, 'J', W. Darling, M. F. 1 lundley, E. J. Peterson, and J. D. Thompson, Phys. Rev. **B** 52, 4926 (1995).
9. T. Caillat, J. -1'. Fleurial, and A. Borshchevsky, Journal of Crystal Growth, accepted for publication (1 995).
10. J. A, McCormack and J. -1'. Fleurial, in Modern Perspectives on Thermoel ectric and Related Materials, edited by D. D. Alred, C. B. Vining and (i, A. Slack (Materials Research Society, Pittsburgh, 1991), p.135.
11, C. Wood, D. Zoltan, and G. Stapfer, Rev. Sci. Instrum. 56, 719 (1 985).
12. J. W. Vandersande, A, Zoltan, and C. Wood, Int. J. of Thermophysics 10,251 (1 989).
13. 1,. Gailliard, '1'. Caillat, H. Scherrer, and S. Scherrer, Proceedings of the VIIIth International Conference on Thermoelectrics, Nancy, France, edited by 11, And S. Scherrer, Institut National Polytechnique de 1 .orraine, Nancy, France (1 988).
14, V. 1.1 istul, *Heavily Doped Semiconductors* (Plenum Press, New York, 1969).
1 S. A, Kjekshus and '1'. Rakke, Acta Chem. Scan. A28, 99 (1974).
1 6. O. L. Anderson, J. Phys. Chem. Solids 24, 909 (1 963).
17. A. Borshchevsky, J. -P. Fleurial, E. Allevato, and '1'. Caillat, in Proceedings of the XIIIth International Conference on Thermoelectrics, Kansas City, MO, USA, edited by B. Mathiprakasam and P. 1 leenan (All' Conference 316, New York), 31 (1 995).
18. 'T', Caillat, J. -P. Fleurial, and A. Borshchevsky (unpublished).
19. '1'. Morelli and G. 1'. Meisner, J. Appl. Phys. 77, 3777 (1995).
20. G. S. Nolas, G. A. Slack, '1'. M. Tritt, and D. '1'. Morelli, *Proceedings of XIVth International Conference on Thermoelectrics*, St. Petersburg, Russia, to be published by M. V. Vedernikov, A. F. Ioffe Physical-Techn ical Institute, 194201, St. Petersburg, Russia (1 996).

TABLE CAPTIONS

'1'able I. Some physical and transport proper ies at room temperature for p-type $CoSb_3$ and p-type $IrSb_3$[3].

Table 11. Room temperature Hall carrier concentration, electrical resistivity, Hall coefficient, Hall mobility, and Seebeck coefficient values for p- and n-type $CoSb_3$ crystals.

FIGURES CAPTIONS

Figure 1. The room temperature Hall mobility values for n- and p-type $CoSb_3$ crystals as a function of the Hall carrier concentration

Figure 2. The room temperature electrical resistivity values for n- and p-type $CoSb_3$ crystals as a function of the Hall carrier concentration

Figure 3. The room temperature Seebeck coefficient values for n- and p-type $CoSb_3$ crystals as a function of the Hall carrier concentration. The dashed lines represent the best-fit of the experimental data.

Figure 4. The power factor (α^2/ρ) values as a function of the Hall carrier concentration for p- and n-type $CoSb_3$ at room temperature

Figure 5. The electrical resistivity values as a function of the inverse temperature for p-type $CoSb_3$

Figure 6. The Hall coefficient values as a function of the inverse temperature for p-type $CoSb_3$.

Figure 7. The electrical resistivity values as a function of the inverse temperature for n-type $CoSb_3$.

Figure 8. The Hall coefficient values as a function of the inverse temperature for n-type $CoSb_3$.

Figure 9. The Hall mobility values as a function of the temperature for p-type $CoSb_3$.

Figure 10. The Hall mobility values as a function of the temperature for n-type $CoSb_3$

Figure 11. The Seebeck coefficient values as a function of the temperature for p-type $CoSb_3$

Figure 12. The Seebeck coefficient values as a function of the temperature for n-type $CoSb_3$

Figure 13. The hole effective mass as a function of the 1 lall carrier concentration at room temperature. The dashed line represents the best-fit curve of the experimental data

Figure 14. The electron effective mass as a function of the I lan carrier concentration at room temperature. The dashed line represents the best-fit curve of the experimental data

Figure 15. The Seebeck coefficient values as a function of the I lall carrier concentration for p-type $CoSb_3$ at room temperature. The solid line represents the best-ilt curve of the experimental data and the dashed line corresponds to the values calculated using the model proposed by Singh and Pickett.[7]

Figure 16. The Seebeck coefficient values as a function of the temperature for selected p-type $CoSb_3$ samples. The solid lines represent the experimental data and the doltcd-dashed line correspond to the values calculated using the mode] proposed by Singh and Pickett.[7]

Figure 17. The hole mobility values as a function of the carrier concentration at room temperature. The solid line represents the calculated values using a single parabolic valence band mode] with acoustic phonon scattering and the dashed line is the $p^{-1/3}$ behavior predicted by Singh and Pickett.[7]

Figure 1 8. X-ray lattice constant as a function of temperature for $CoSb_3$

Figure 19. The thermal conductivity values as a function of the temperature for n-type $CoSb_3$. The calculated lattice thermal conductivity values arc also Shown,

Property	Units	p-type $IrSb_3$	p-type $CoSb_3$
Lattice constant	Å	9.2503	9.0345
X-ray density	g/cm^3	9.356	7.621
Experimental density	g/cm^3	9.16	7.582.
Decomposition temperature	K	1414	1146
Shear sound velocity	105 cm/s	4.675	4.590
Transversal sound velocity	105 cm/s	2.717	2.643
Debye temperature	K	308	307
Thermal expansion coefficient	10^{-6} K	6.6	6.36
Grüneisen constant		1.42.	0.952
Electrical resistivity	mΩ.cm	0.429	1.894
Hall mobility	$cm^2/V\ s$	1320	2835
Hall carrier concentration	$10^{19}/cm^3$	1.1	0.116
Seebek coefficient	μV/K	72	220
Lattice thermal conductivity	mW/cm K	160	100
Effective mass (m^*/m_0)		0.17	0.153
Band gap	ev	1,4	0.5s

Table I

Sample	Conductivity type	Carrier concentration (cm^{-3})	Electrical resistivity (mΩcm)	Hall coefficient (cm^3/C)	Hall mobility (cm^2/Vs)	Seebeck coefficient (μV/K)
121 OEW2	P	1.21E+17	17.360	51.59	2972.0	280.0
10OB22	P	4.39E+17	5.303	14,21	2679.0	240.0
71NB13	P	1.16E+18	1.894	5,37	2835.7	220.0
23NB12	P	1.51E+18	1.596	4.14	2596.0	179.0
2NB13	P	3.89E+18	0.812	1.61	1981.0	139.0
3NB13	P	4.37E+18	0.737	1.43	1944.0	138.0
2NB9	P	9.45E+18	0.432	0.66	15?8.0	80.0
1CS1O (0.08 at% Te)	n	4.54E+18	14.20	1.37	101.0	-452.0
1CS7 (0.1 at% Te)	n	4.94E+18	11.64	1.27	108.8	-443.0
1CS11 (0.15 at% Te)	n	1.29E+19	5.57	0.49	87.0	-373.0
2CS9 (0.12 at% Te)	n	1.52E+19	5.99	0.41	68.0	-364.0
4OB25 (0.6 at% Pd)	n	4.41E+19	3.80	0.14	37.2	-280.0
OB26 (1 at% Pd)	n	1.38E+20	1.10	0.05	41.2	-180.0

Table II

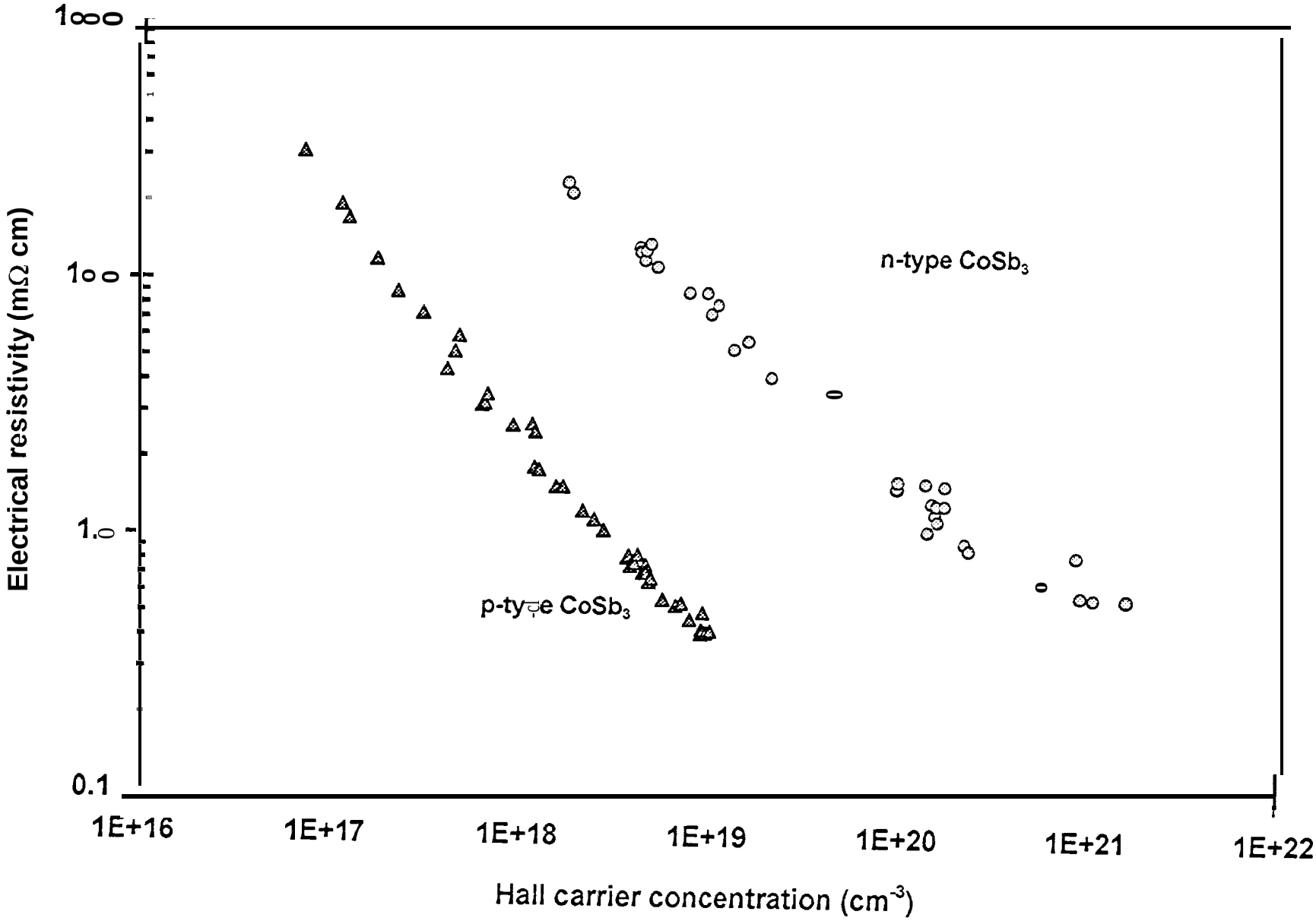
1000
100
10
1
0.1
Electrical resistivity (mΩ cm)
1E+16
1E+17
1E+18
1E+19
1E+20
1E+21
1E+22
Hall carrier concentration (cm-3)
n-type CoSb3
p-type CoSb3

Figure 2

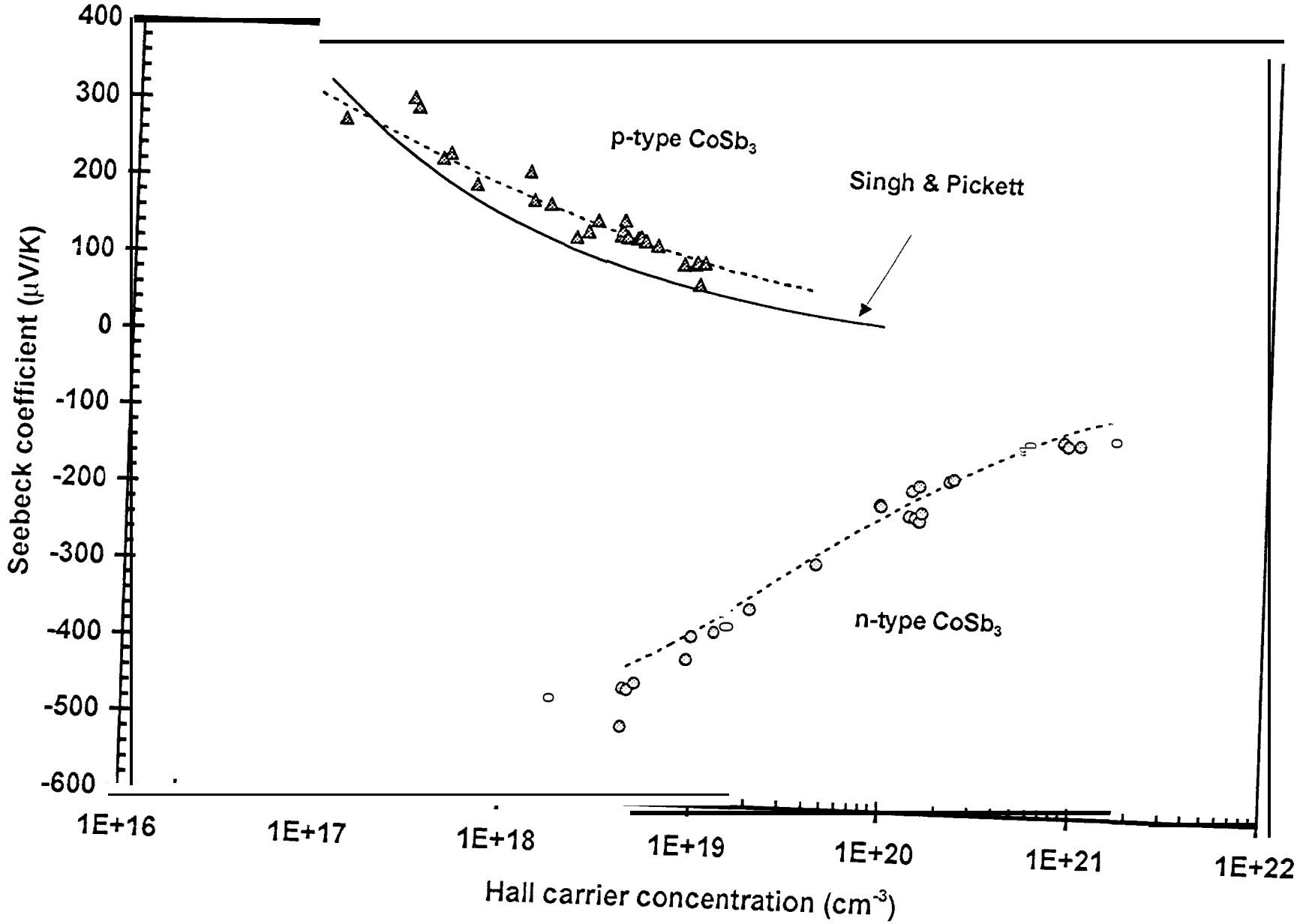
400
300
200
100
0
-100
-200
-300
-400
-500
-600
Seebeck coefficient (μV/K)
p-type CoSb3
Singh & Pickett
n-type CoSb3
1E+16
1E+17
1E+18
1E+19
1E+20
1E+21
1E+22
Hall carrier concentration (cm-3)

Figure 3

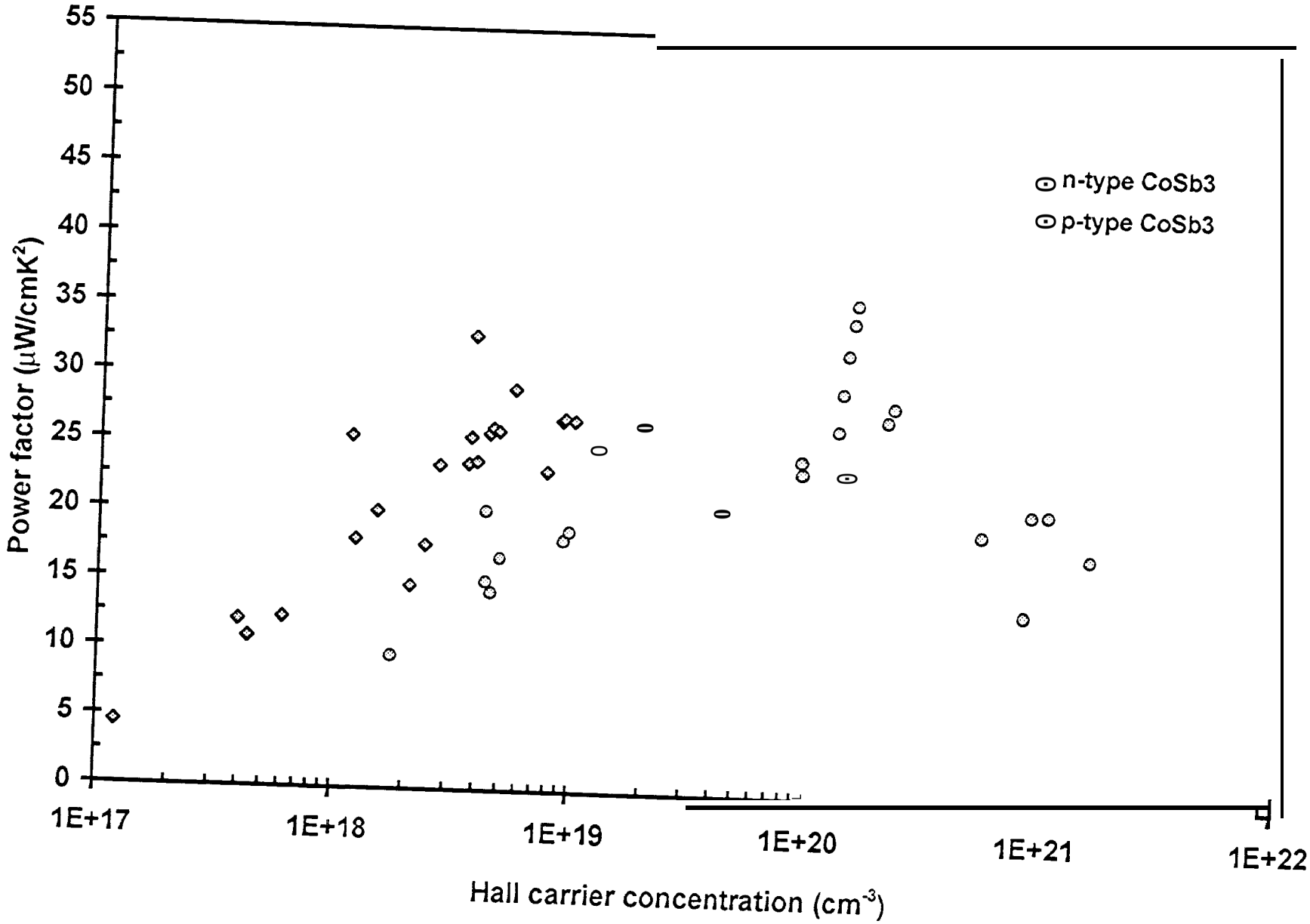
55
50
45
40
35
30
25
20
15
10
5
0
Power factor (μW/cmK²)
1E+17
1E+18
1E+19
1E+20
1E+21
1E+22
Hall carrier concentration (cm⁻³)
n-type CoSb3
p-type CoSb3

Figure 4

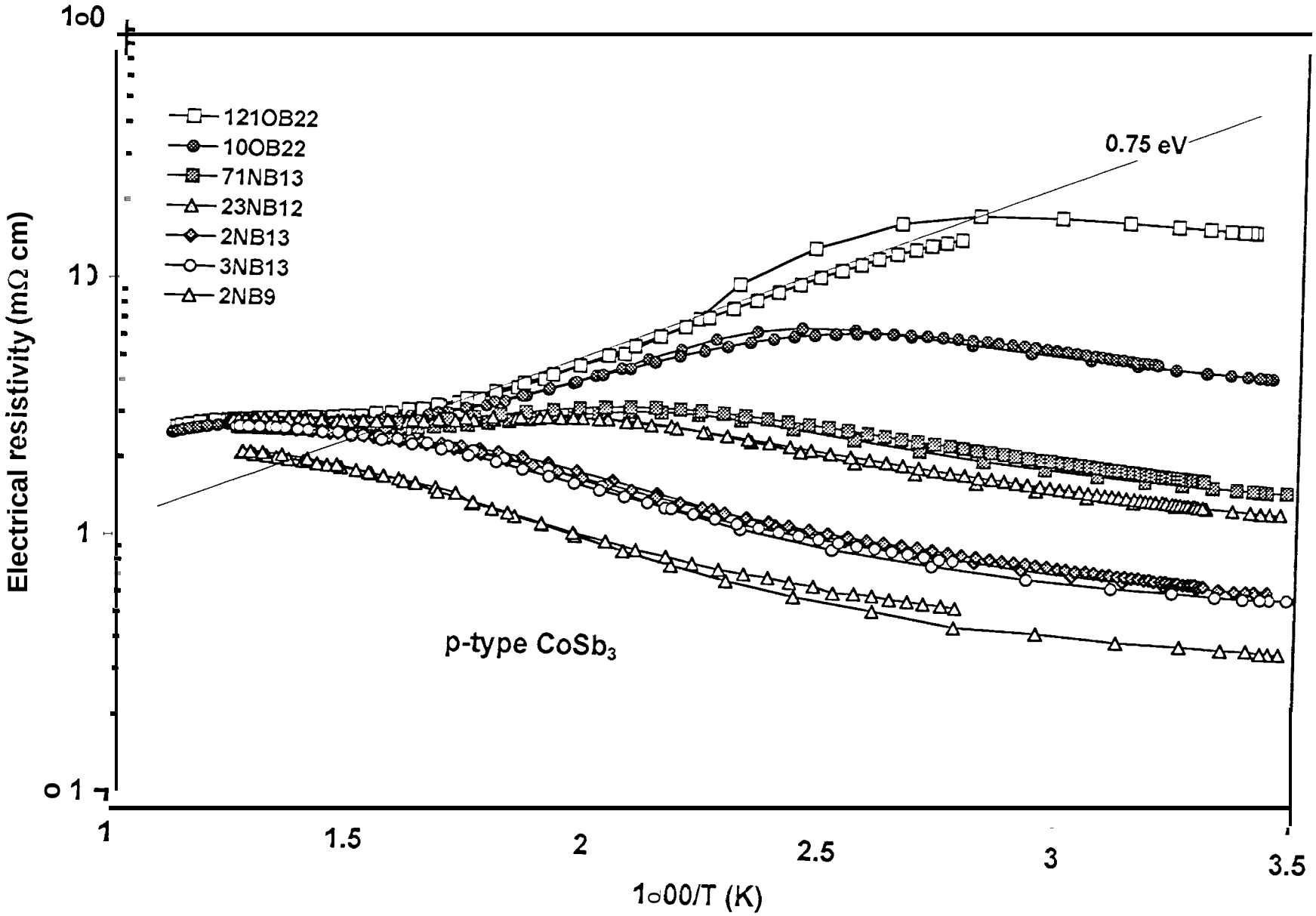
100
10
1
0.1
Electrical resistivity (mΩ cm)
121OB22
10OB22
71NB13
23NB12
2NB13
3NB13
2NB9
0.75 eV
p-type CoSb3
1
1.5
2
2.5
3
3.5
1000/T (K)

Figure 5

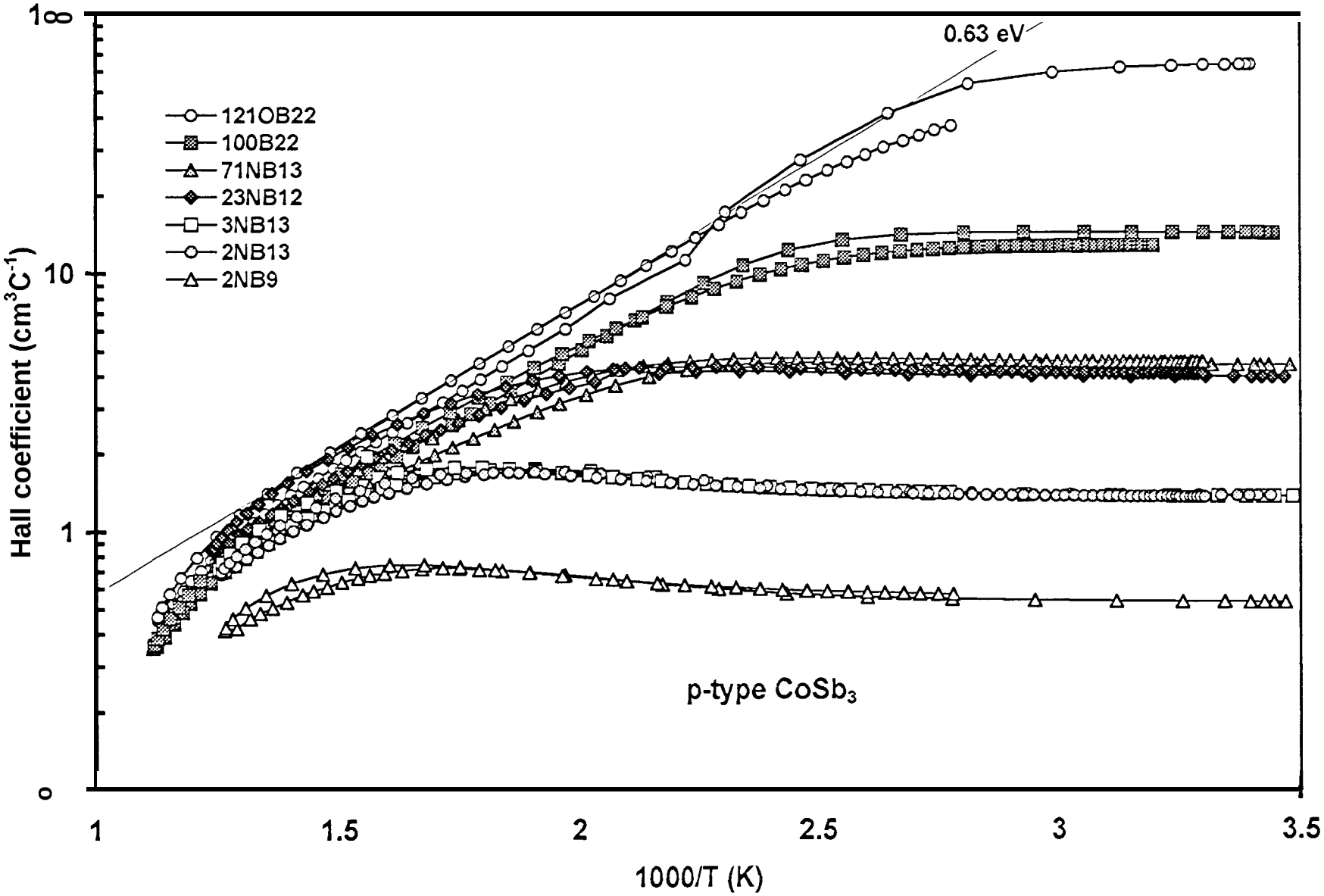
0.63 eV
121OB22
100B22
71NB13
23NB12
3NB13
2NB13
2NB9
p-type $CoSb_3$
Hall coefficient (cm^3C^{-1})
100
10
1
0
1
1.5
2
2.5
3
3.5
1000/T (K)

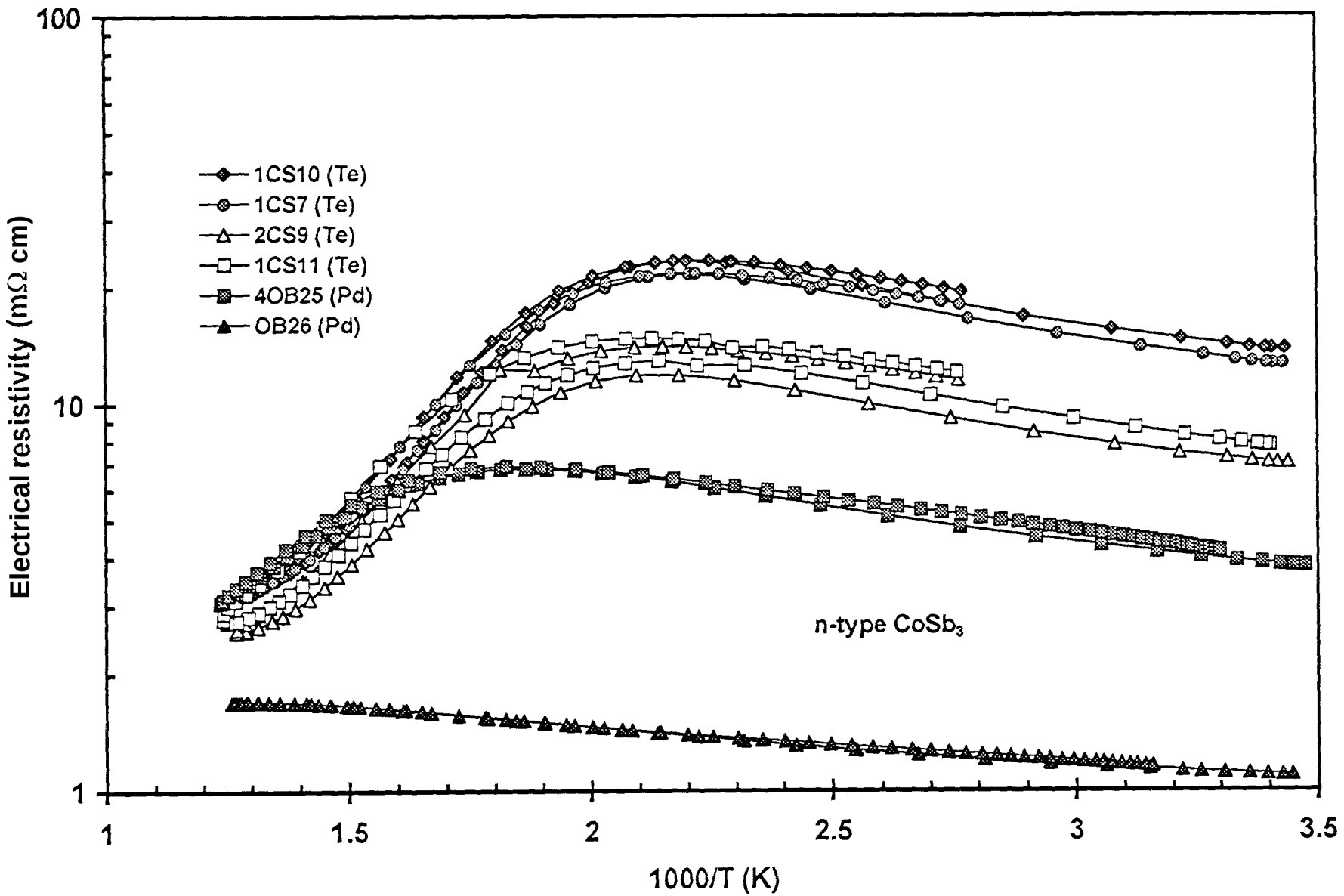
100
10
1
Electrical resistivity (mΩ cm)
1CS10 (Te)
1CS7 (Te)
2CS9 (Te)
1CS11 (Te)
4OB25 (Pd)
OB26 (Pd)
n-type CoSb3
1
1.5
2
2.5
3
3.5
1000/T (K)

Figure 7

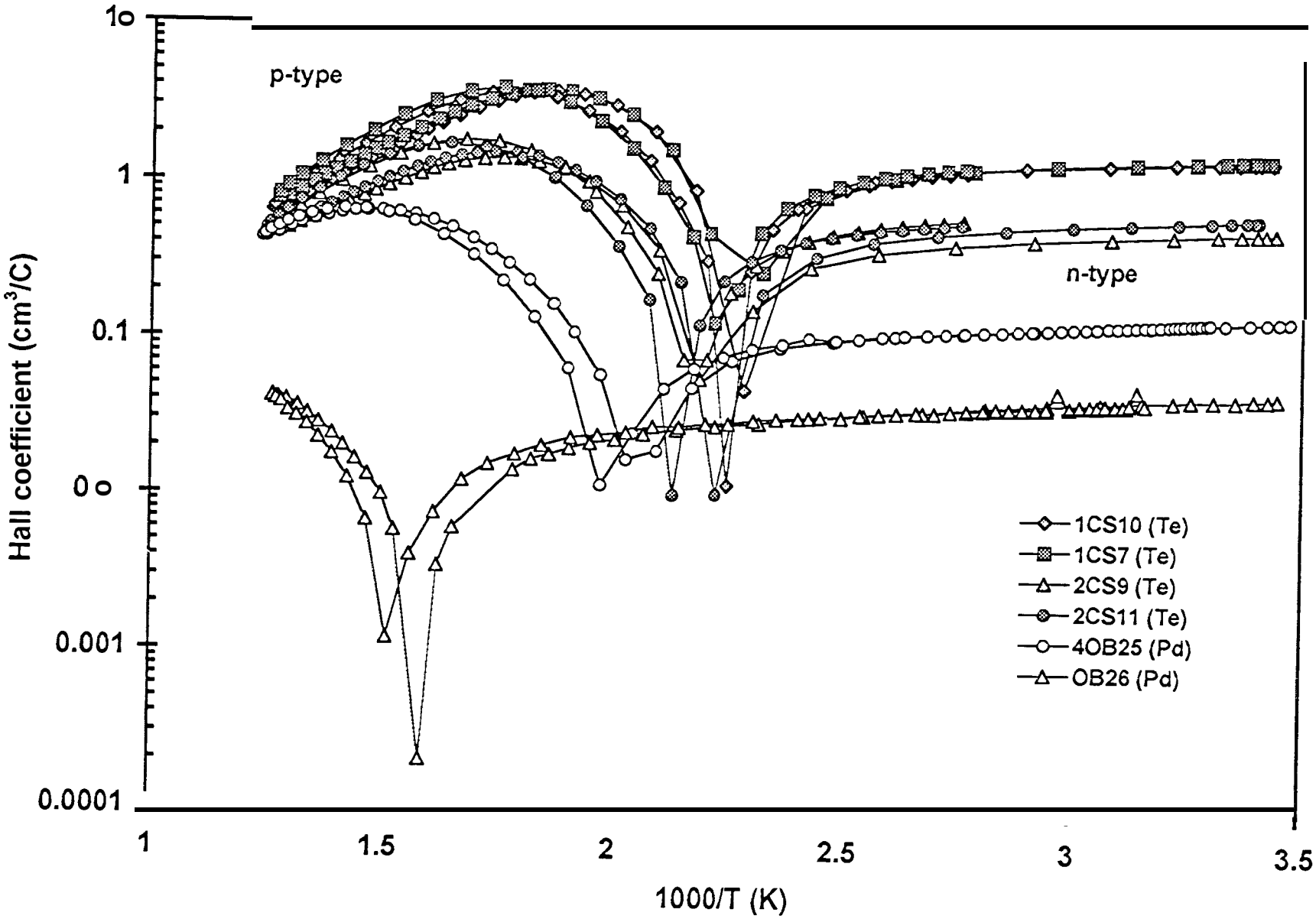
10
1
0.1
0.0
0.001
0.0001
Hall coefficient (cm³/C)
p-type
n-type
1CS10 (Te)
1CS7 (Te)
2CS9 (Te)
2CS11 (Te)
4OB25 (Pd)
OB26 (Pd)
1
1.5
2
2.5
3
3.5
1000/T (K)

Figure 8

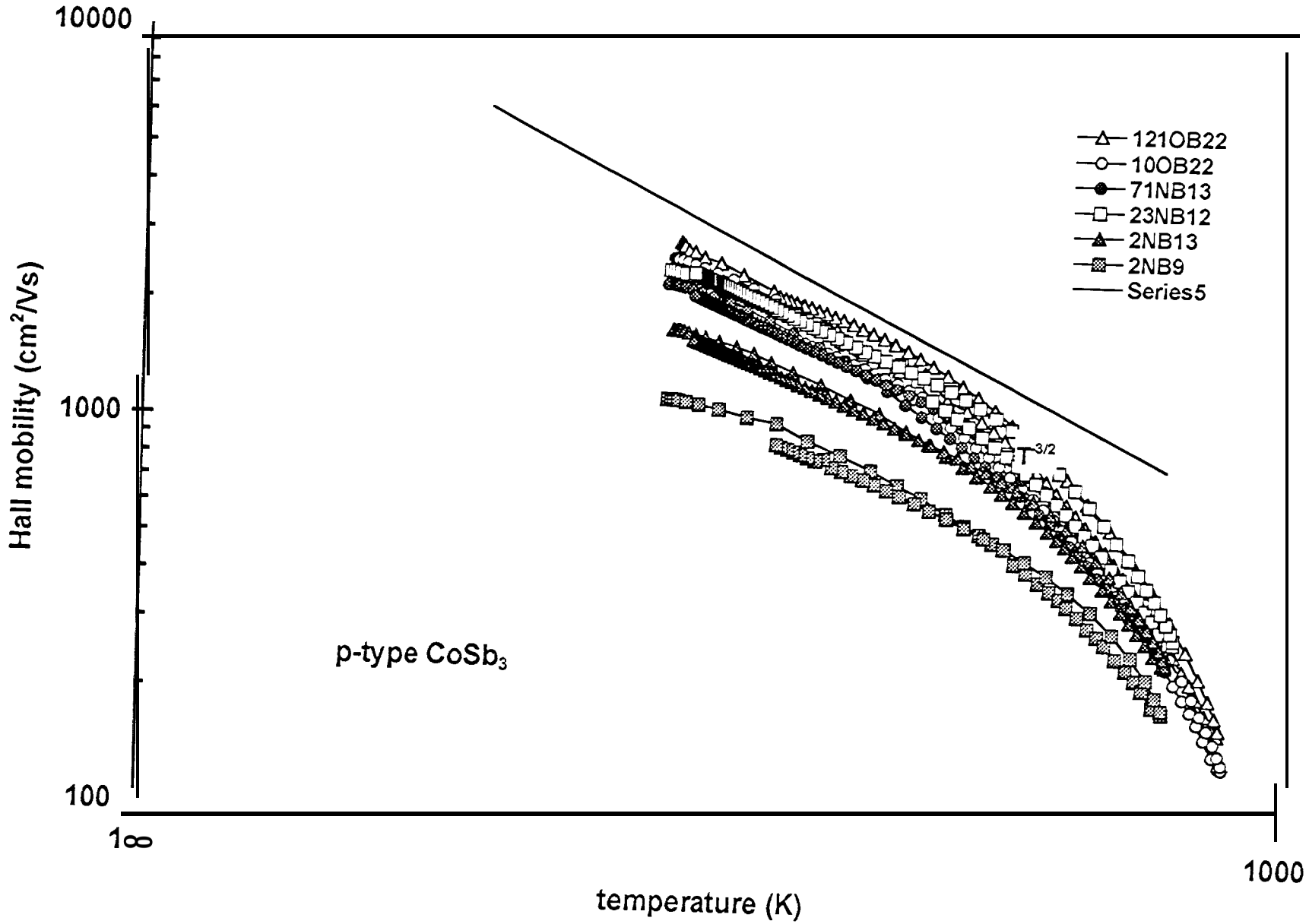
10000
1000
100
Hall mobility (cm²/Vs)
p-type CoSb3
T-3/2
121OB22
10OB22
71NB13
23NB12
2NB13
2NB9
Series5
10
1000
temperature (K)

Figure 9

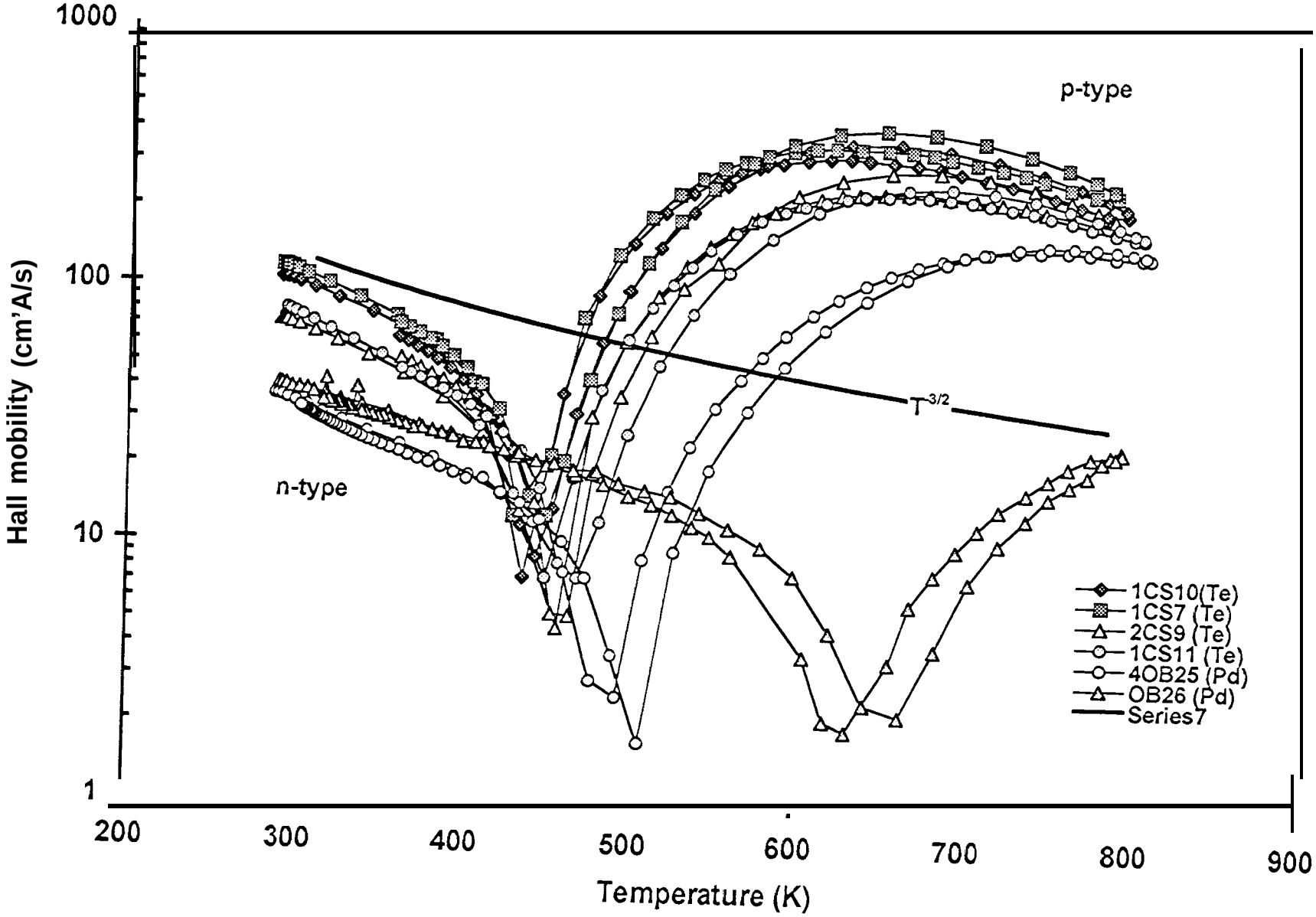
1000
100
10
1
Hall mobility (cm'A/s)
200
300
400
500
600
700
800
900
Temperature (K)
p-type
n-type
T^3/2
1CS10(Te)
1CS7 (Te)
2CS9 (Te)
1CS11 (Te)
4OB25 (Pd)
OB26 (Pd)
Series7

F g 0

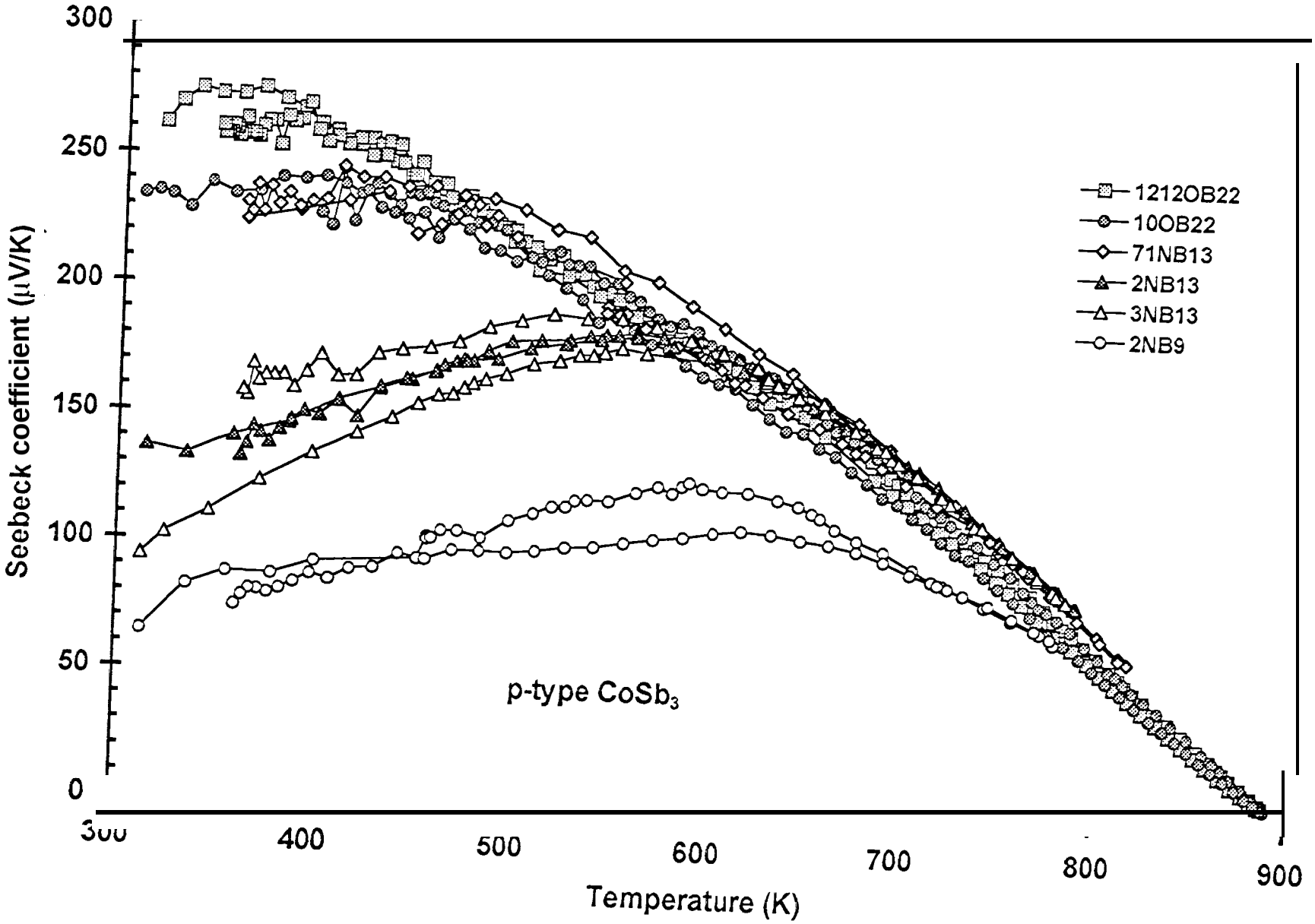
300
250
200
150
100
50
0
Seebeck coefficient (μV/K)
300
400
500
600
700
800
900
Temperature (K)
1212OB22
10OB22
71NB13
2NB13
3NB13
2NB9
p-type CoSb3

Figure 11

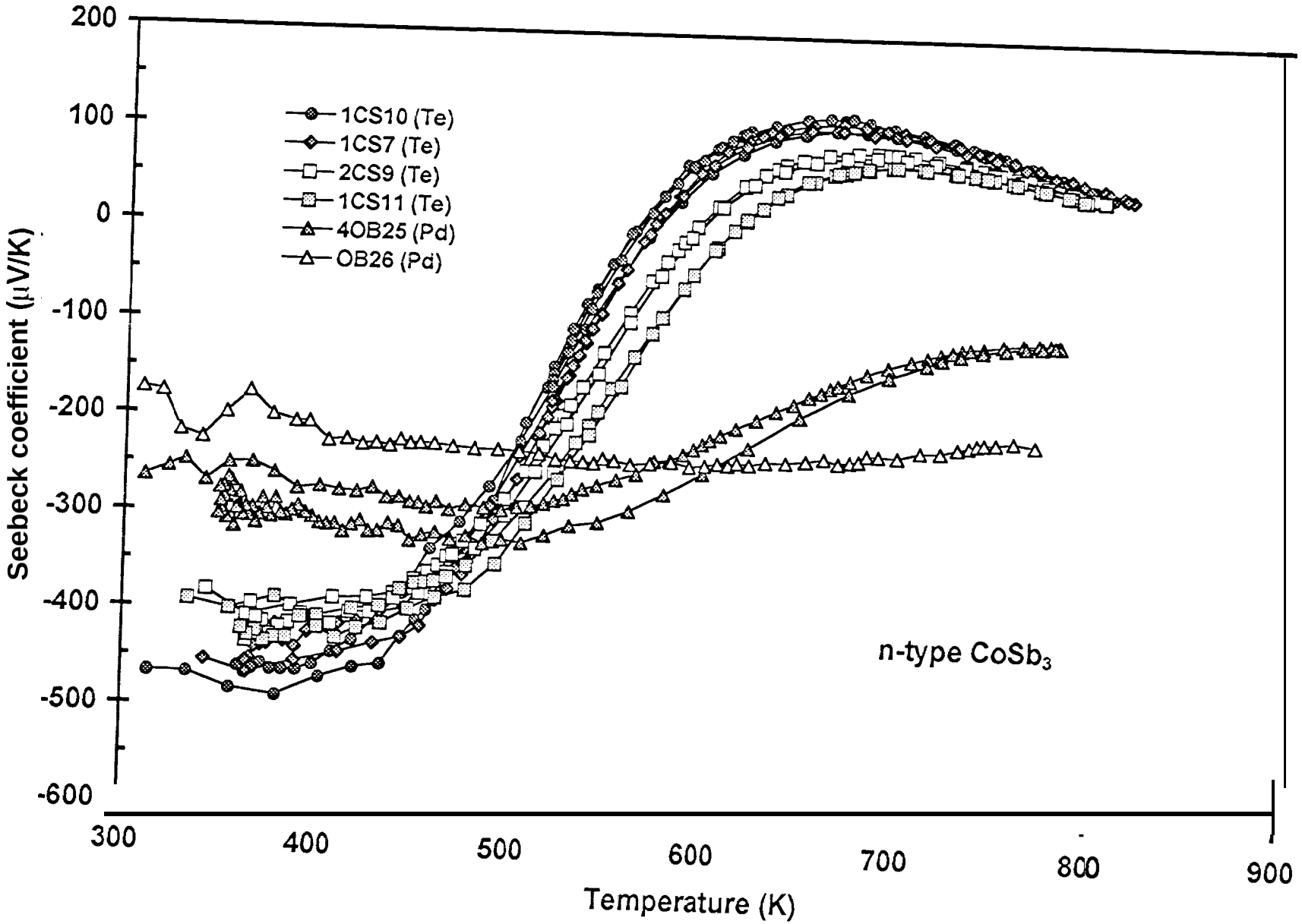
200
100
0
-100
-200
-300
-400
-500
-600
Seebeck coefficient (μV/K)
1CS10 (Te)
1CS7 (Te)
2CS9 (Te)
1CS11 (Te)
4OB25 (Pd)
OB26 (Pd)
n-type CoSb3
300
400
500
600
700
800
900
Temperature (K)

Fig 2

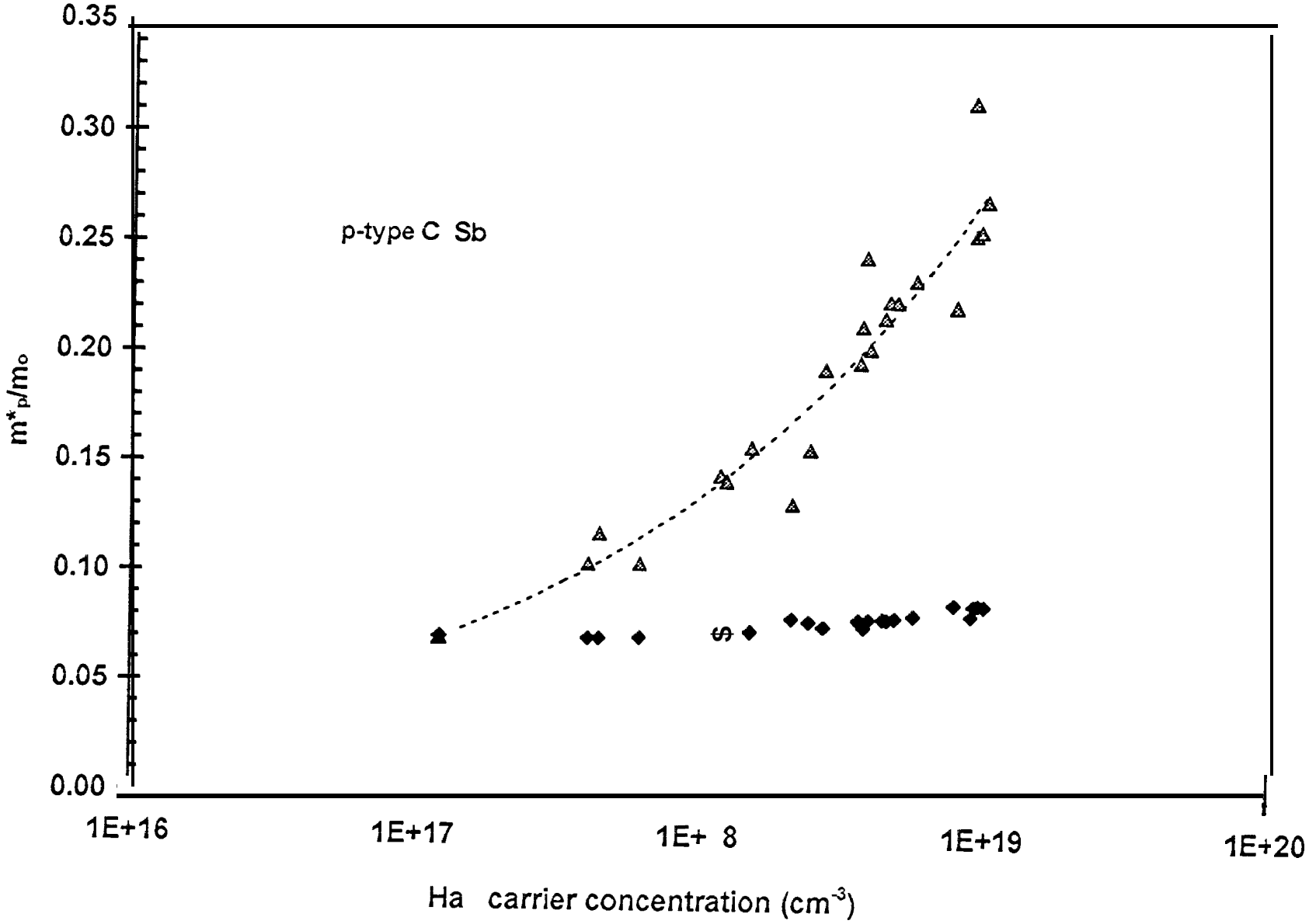
0.35
0.30
0.25
0.20
0.15
0.10
0.05
0.00
m*p/mo
p-type C Sb
1E+16
1E+17
1E+ 8
1E+19
1E+20
Ha carrier concentration (cm-3)

Figure 13

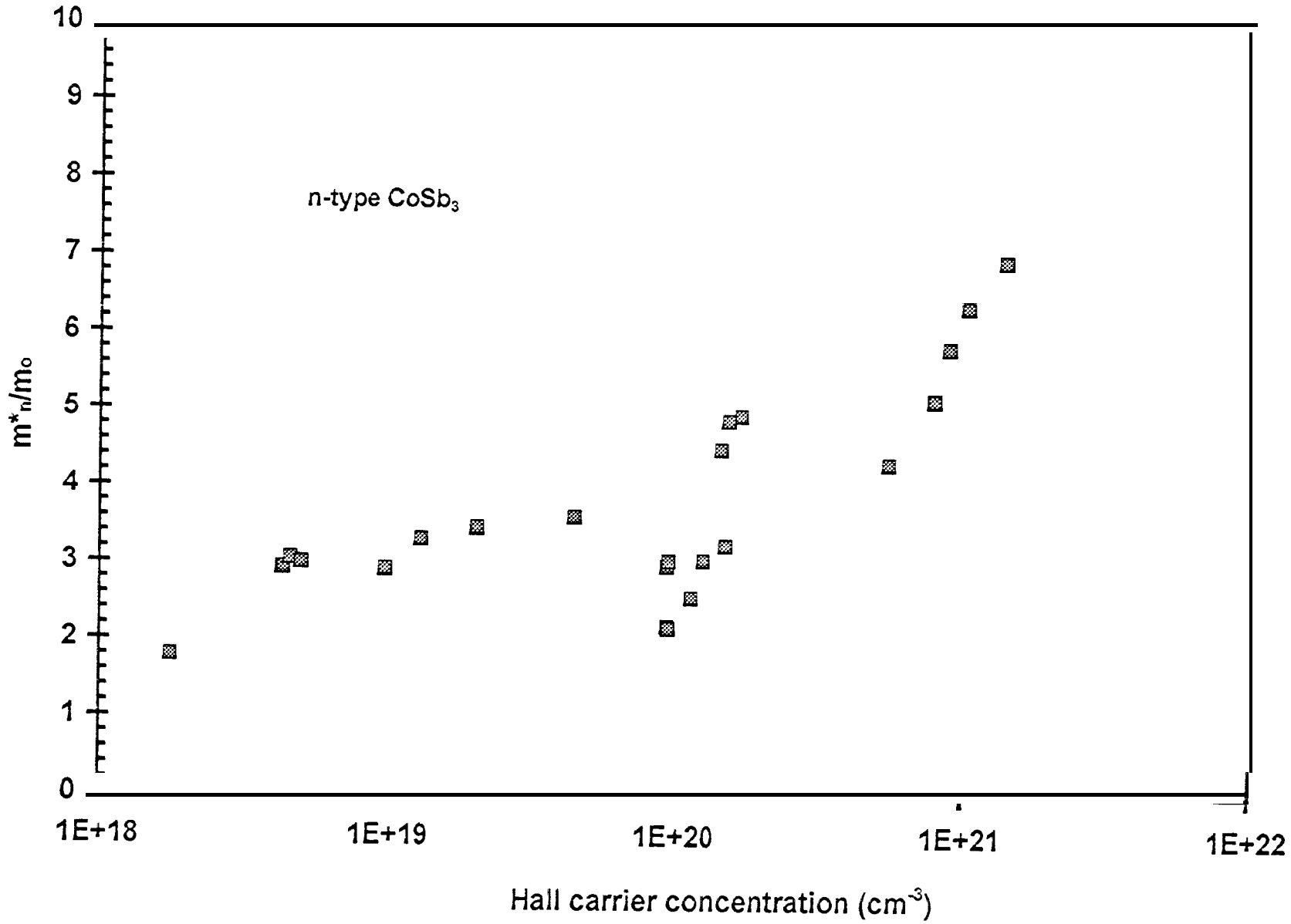
n-type CoSb3
m*n/mo
10
9
8
7
6
5
4
3
2
1
0
1E+18
1E+19
1E+20
1E+21
1E+22
Hall carrier concentration (cm-3)

Figure 14

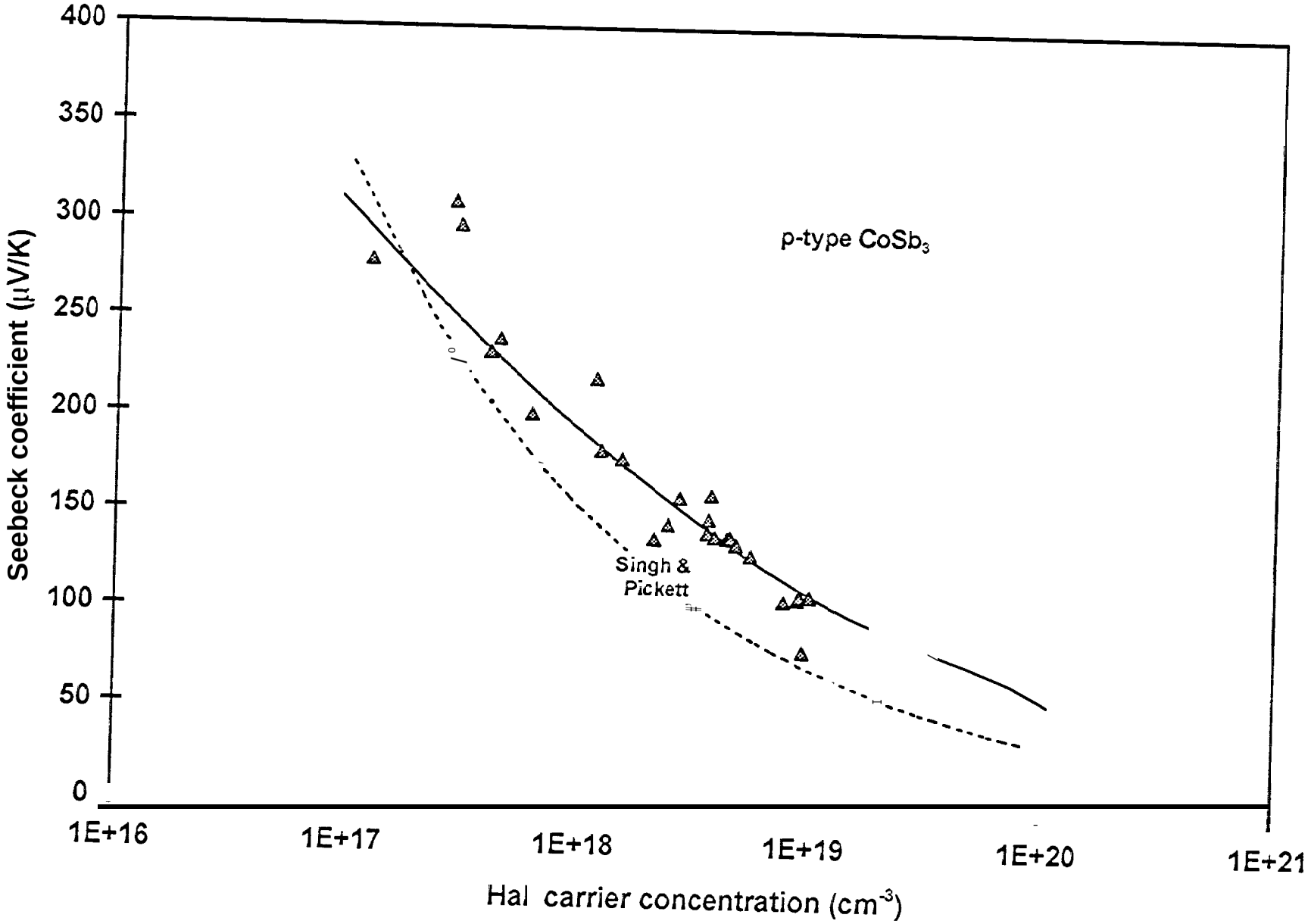
400
350
300
250
200
150
100
50
0
Seebeck coefficient (μV/K)
p-type CoSb3
Singh &
Pickett
1E+16
1E+17
1E+18
1E+19
1E+20
1E+21
Hal carrier concentration (cm-3)

Figure 15

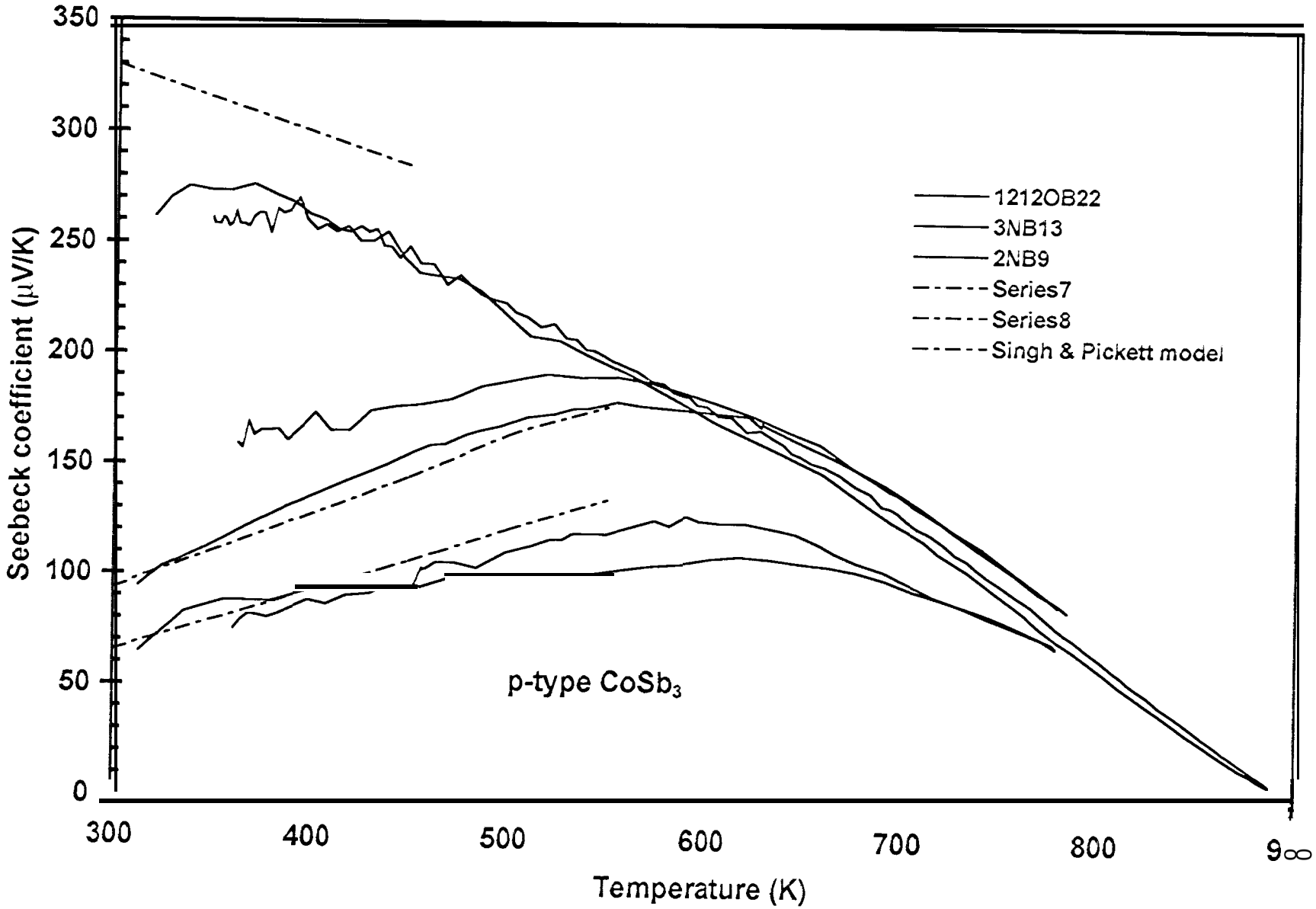
350
300
250
200
150
100
50
0
Seebeck coefficient (μV/K)
300
400
500
600
700
800
900
Temperature (K)
1212OB22
3NB13
2NB9
Series7
Series8
Singh & Pickett model
p-type CoSb3

Figure 16

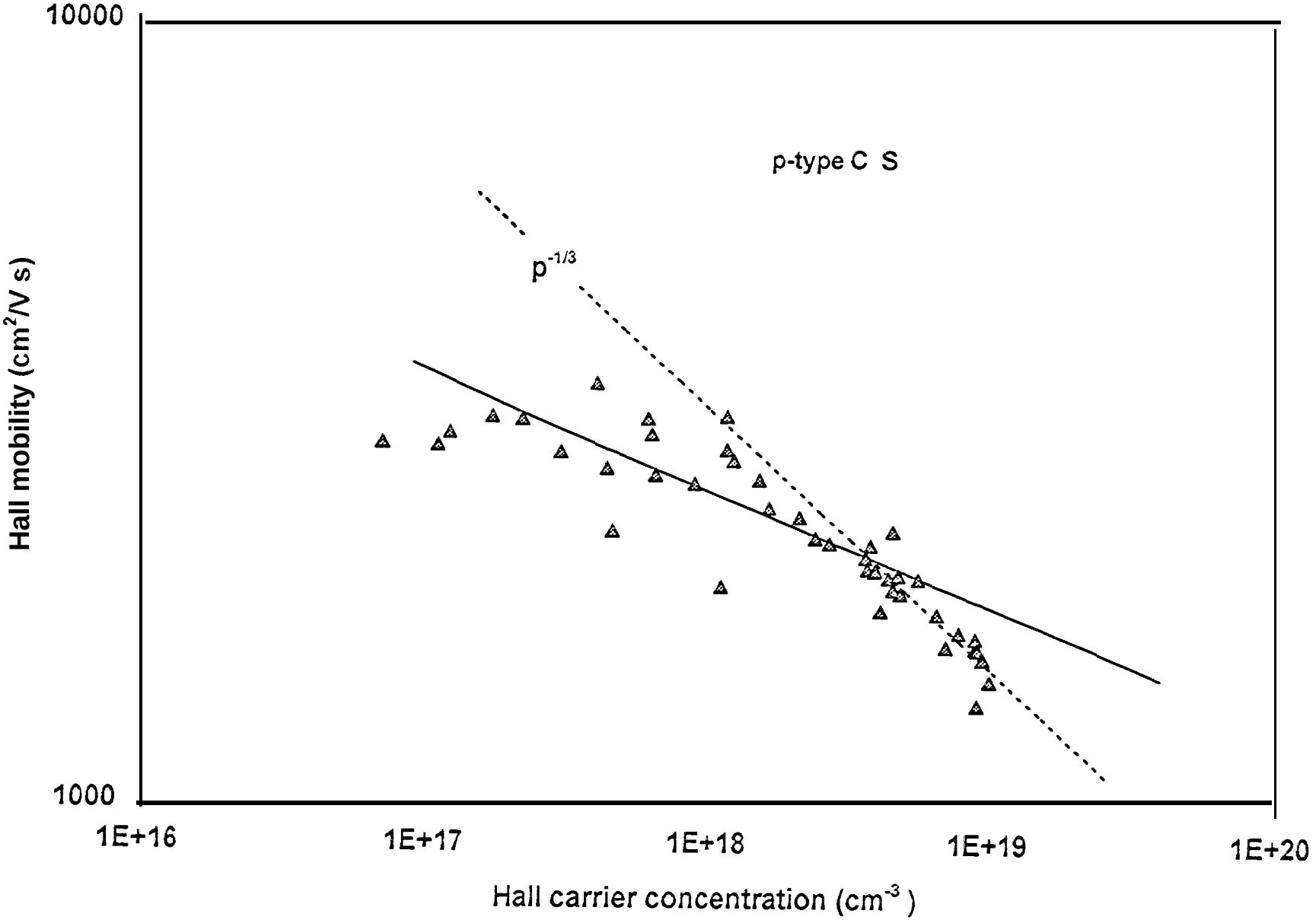
10000
1000
Hall mobility (cm²/V s)
p-type C S
p^-1/3
1E+16
1E+17
1E+18
1E+19
1E+20
Hall carrier concentration (cm^-3)

Figure 17

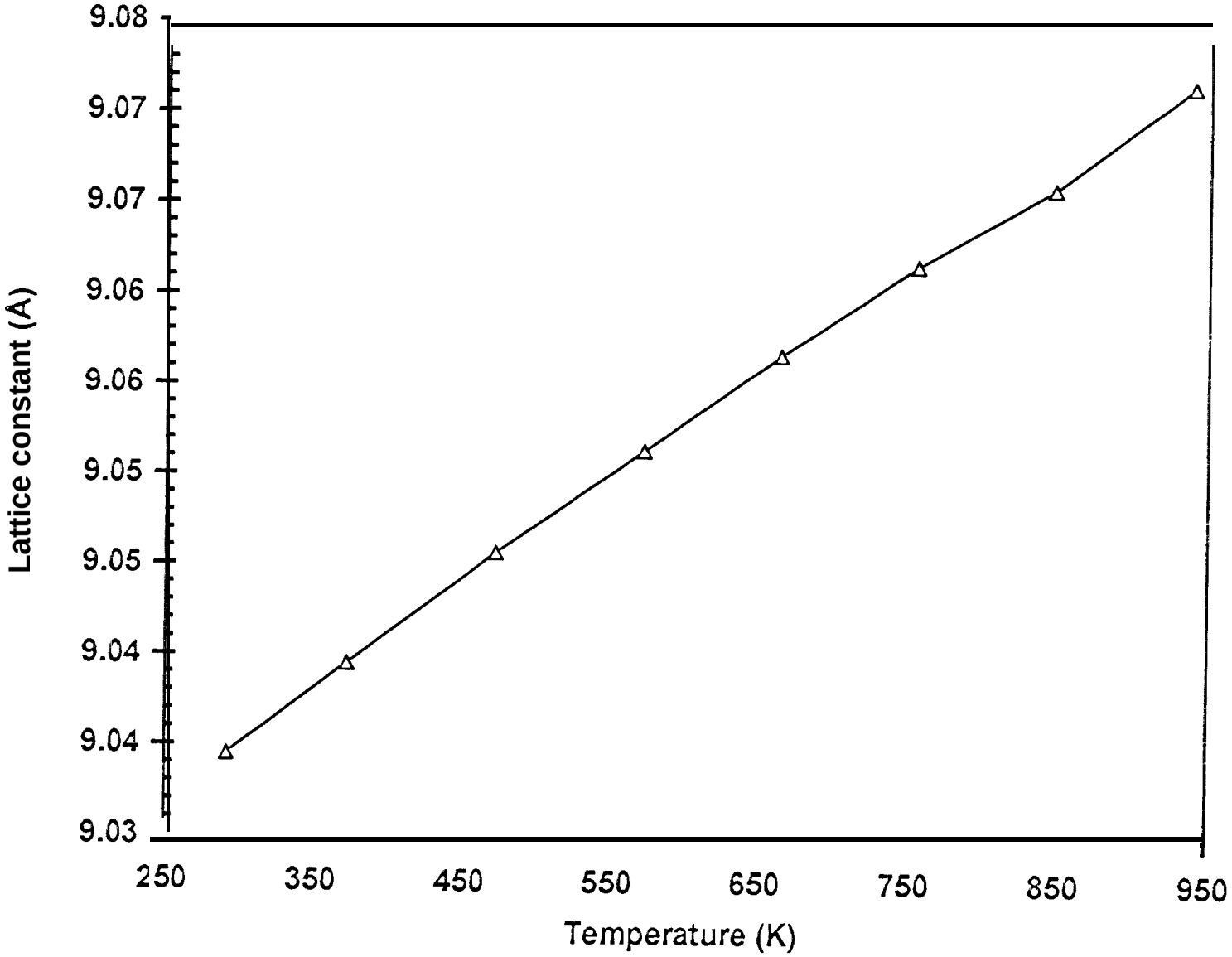
9.08
9.07
9.07
9.06
9.06
9.05
9.05
9.04
9.04
9.03
Lattice constant (A)
250
350
450
550
650
750
850
950
Temperature (K)

Figure 18

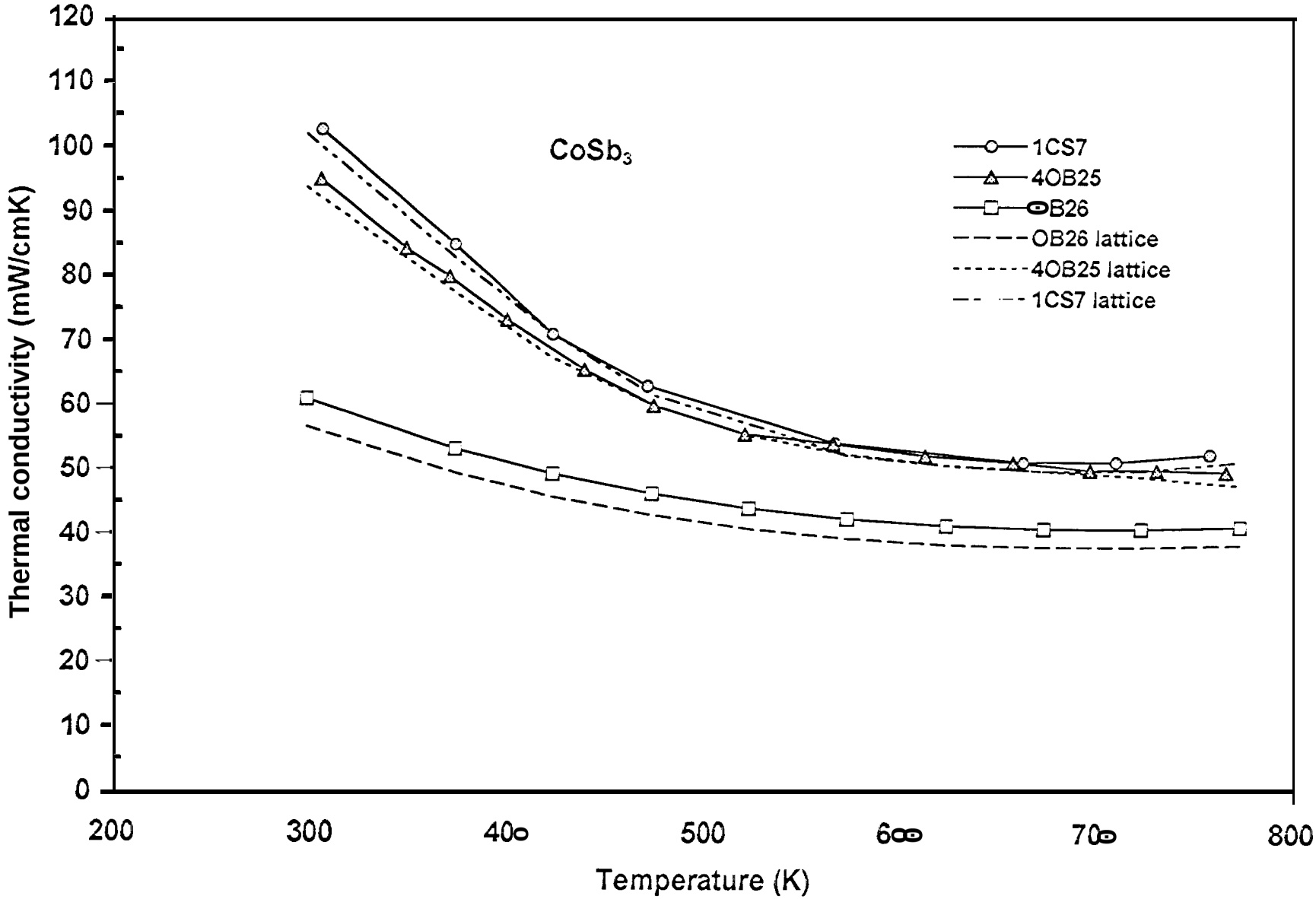
CoSb3
1CS7
4OB25
OB26
OB26 lattice
4OB25 lattice
1CS7 lattice
Thermal conductivity (mW/cmK)
Temperature (K)
0
10
20
30
40
50
60
70
80
90
100
110
120
200
300
400
500
600
700
800